Bioorganic & Medicinal Chemistry 20 (2012) 2950–2956

Contents lists available at SciVerse ScienceDirect

Bioorganic & Medicinal Chemistry

journal homepage: www.elsevier.com/locate/bmc

Molecular docking and enzymatic evaluation to identify selective inhibitors of aspartate semialdehyde dehydrogenase

Amarjit Luniwal [a,b], Lin Wang [a], Alexander Pavlovsky [a], Paul W. Erhardt [b], Ronald E. Viola [a,*]

[a] Department of Chemistry, University of Toledo, Toledo, OH 43606, USA
[b] Center for Drug Design and Development, University of Toledo, Toledo, OH 43606, USA

ARTICLE INFO

Article history:
Received 19 January 2012
Revised 26 February 2012
Accepted 5 March 2012
Available online 10 March 2012

Keywords:
Aspartate semialdehyde dehydrogenase
Docking models
Virtual screening
Enzyme inhibitors
Validation

ABSTRACT

Microbes that have gained resistance against antibiotics pose a major emerging threat to human health. New targets must be identified that will guide the development of new classes of antibiotics. The selective inhibition of key microbial enzymes that are responsible for the biosynthesis of essential metabolites can be an effective way to counter this growing threat. Aspartate semialdehyde dehydrogenases (ASADHs) produce an early branch point metabolite in a microbial biosynthetic pathway for essential amino acids and for quorum sensing molecules. In this study, molecular modeling and docking studies were performed to achieve two key objectives that are important for the identification of new selective inhibitors of ASADH. First, virtual screening of a small library of compounds was used to identify new core structures that could serve as potential inhibitors of the ASADHs. Compounds have been identified from diverse chemical classes that are predicted to bind to ASADH with high affinity. Next, molecular docking studies were used to prioritize analogs within each class for synthesis and testing against representative bacterial forms of ASADH from *Streptococcus pneumoniae* and *Vibrio cholerae*. These studies have led to new micromolar inhibitors of ASADH, demonstrating the utility of this molecular modeling and docking approach for the identification of new classes of potential enzyme inhibitors.

1. Introduction

The development of microbial resistance against many of the front-line antibiotics is a major emerging challenge to human health. Bacterial genus, including *Staphylococcus*, *Streptococcus*, and *Enterococcus*, that were formally susceptible to several classes of antibiotics now exhibit multidrug resistance.[1] Targeting key enzymes, such as those that play crucial roles in the biosynthesis of essential metabolites, can provide a new and effective approach to counter antimicrobial drug resistance. Aspartate semialdehyde dehydrogenase (ASADH) catalyzes an early branch point reaction in a microbial biosynthetic pathway both for essential amino acids and for quorum sensing molecules.[2] Inhibition of ASADH is fatal to microorganisms,[3] and the gene that encodes ASADH has been shown to be part of the minimal set of genes that are essential for life.[4,5] Selective inhibition of this key enzyme can produce lead compounds that could play a role in combating the growing threat from multidrug-resistant infectious organisms.

The structure of this essential metabolic enzyme has been determined from a wide variety of microorganisms, including Gram-negative[6–8] and Gram-positive bacteria,[9] fungal[10] and archael species.[11] The catalytic mechanism of ASADH is supported by kinetic studies,[12,13] mutagenesis studies[14–16] and structural characterization of several key catalytic intermediates.[8,9] Our molecular level understanding of the structural and mechanism of ASADH is being used to guide the identification of selective enzyme inhibitors. In addition, subtle differences between several members of this homologous enzyme family are guiding the future development of species-selective ASADH inhibitors.

Virtual screening has been successfully used as an efficient alternative to high throughput screening approaches for the discovery and development of new compounds.[17] Molecular modeling and docking studies have identified new chemical entities that were then tested against representative ASADHs. These docking models were also used for virtual screening of a small library of commercially available structures to identify compounds with a high potential for selective ASADH inhibition. This combined approach has now led to several new, reasonably potent inhibitors.

2. Results and discussion

2.1. Molecular modeling and docking studies

The high resolution X-ray coordinates for a representative gram-positive (*sp*ASADH)[9] and a gram-negative (*vc*ASADH)[7] bacterial form of ASADH were used for molecular modeling studies, and for comparative analysis of their respective active sites. Many of

* Corresponding author. Tel.: +1 419 530 1582; fax: +1 419 530 1583.
E-mail address: ron.viola@utoledo.edu (R.E. Viola).

0968-0896/$ - see front matter © 2012 Elsevier Ltd. All rights reserved.
http://dx.doi.org/10.1016/j.bmc.2012.03.013

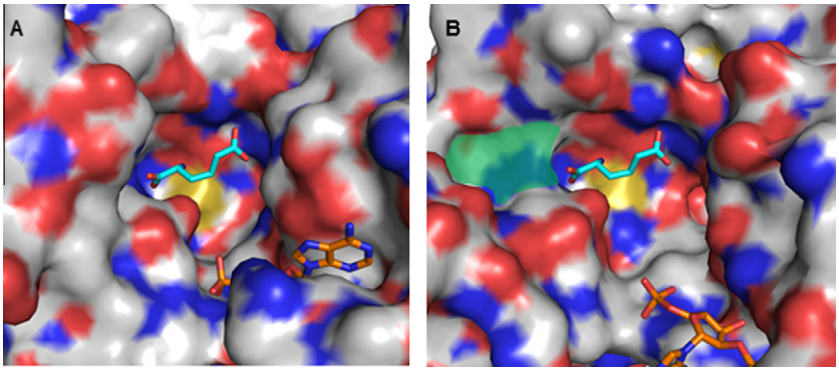

Figure 1. Binding of 2-aminoadipate (cyan) and NADP (orange) in the active site of ASADH. (A) Gram-positive (*S. pneumoniae*) with an additional loop present only in *sp*ASADH; (B) Gram-negative (*V. cholerae*). Note the extra pocket (shaded in green) adjacent to the active site in *vc*ASADH.

the key residues within the active sites of this enzyme family are identical across all of the microbial species that have been examined. However, careful analysis has revealed subtle differences between the active sites of the ASADHs from different bacterial species. In particular, *vc*ASADH has a pocket adjacent to the substrate binding site (Fig. 1B) that is not present in *sp*ASADH because the latter enzyme has an additional loop in this locale composed of amino acids 191–198 (Fig. 1A). The absence of this loop in *vc*ASADH provides some 'extra space' in this region of the structure. These differences have been exploited in the modeling, design and testing of potential inhibitors in order to gain selectivity between these two enzyme orthologs.

The performance and predictability of the docking models were examined by using both internal and external validation of the potential inhibitory ligand-active site complexes. For internal validation, the top docking score pose of the known inhibitor 2-aminoadipate (2-aa) was superimposed over the X-ray coordinates of the experimentally derived structure of this inhibitor bound to *sp*ASADH.[18] The docking pose of 2-aa is oriented similarly to the electron density of this bound inhibitor (Fig. 2). The docked and actual inhibitor structures superimpose quite well with an RMSD of 0.46 Å, well within commonly acceptable limits.[19] In particular, the α-carboxylate group of 2-aa engages in hydrogen-bonding interactions with R245, and the γ-carboxylate interacts with R99 in both the docked and experimental structures, validating the capability of these docking studies to predict an experimentally determined structure.

To examine the broader predictability of the docking models, a training data set of more structurally diverse compounds (Fig. 3) were chosen from a group of inhibitors with known binding affinities for the ASADHs from both *Vibrio cholerae* and *Streptococcus pneumoniae*.[18] Correlations between measured binding affinities and the predicted affinities for each compound were assessed for various docked models. A comparative analysis of the experimental and predicted activities was performed to establish the predictive capability of this approach. The docking models demonstrate reasonably good predictive power, as indicated by the correlation between the experimental and predicted binding affinities of the training set molecules. The cross-validation correlation coefficient (r^2) values were 0.9 for *sp*ASADH (Fig. 4A) and 0.7 for *vc*ASADH (Fig. 4B).

2.1.1. Library selection

Based on our detailed understanding of the architecture of the ASADH active site and the availability of high resolution structural data for several inhibitors bound to *sp*ASADH,[18] an intuitive search for available inhibitor mimic structures was conducted using SciFinder. Beginning with a large library of potential compounds,

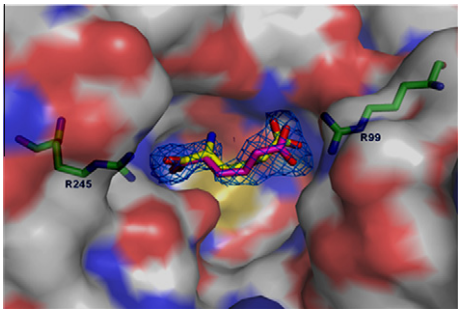

Figure 2. Docking model generated pose (in yellow) of 2-aminoadipate bound to *sp*ASADH compared to its experimentally determined coordinates and electron density obtained by X-ray (in magenta). In both the docked and experimental structures the carboxyl groups of the inhibitor make electrostatic interactions with the active site arginyl groups (R99 and R245).

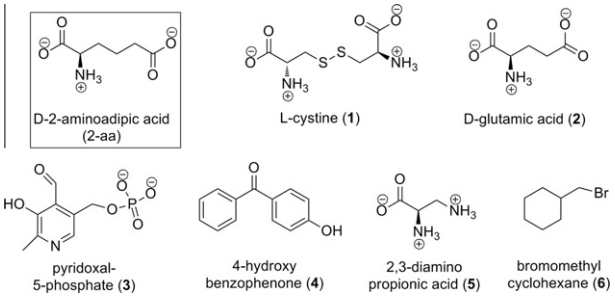

Figure 3. Structures of external validation training set obtained from known inhibitors of ASADHs, compared to the structure of 2-aminoadipate.

we were able to significantly narrow the search by using our current detailed understanding of the enzyme and several selection criteria as filters. The primary criteria used were to identify analogs with at least two functional moieties that are able to establish electrostatic interactions with the key active site arginine residues. Additionally, these two pharmacophores should be separated by 3–5 bonds to allow them to potentially bridge between the arginines and ideally one of these functional groups should be a good mimic of the phosphate substrate. Because the goal is to elaborate the most promising of these inhibitors into more selective lead compounds, the initial compounds obtained based upon these criteria were further filtered by limiting the choices to those containing aromatic moieties that are more amicable to synthetic manipulations such as coupling to other orthogonally binding fragments.

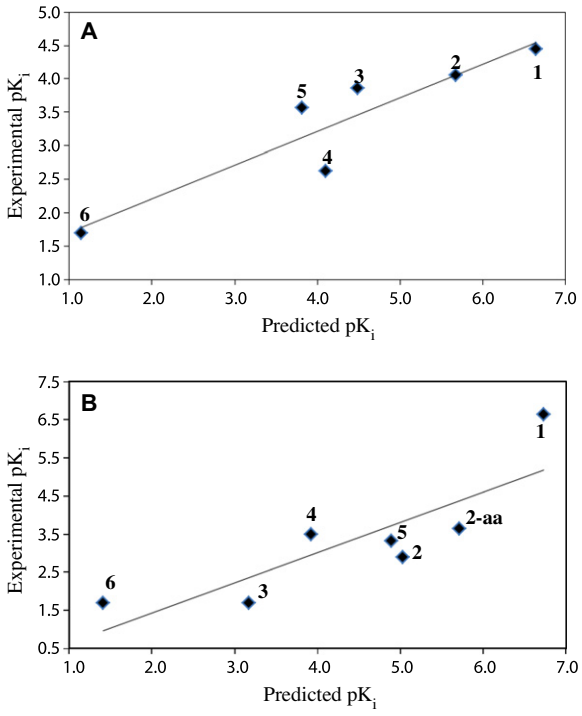

Figure 4. Correlation between the experimental and predicted pK_i values for this set of six known inhibitors of ASADHs. (A) Binding to *sp*ASADH and (B) binding to *vc*ASADH.

2.1.2. Virtual screening and testing

The validated docking models were used for virtual screening of a fragment library of low molecular weight compounds to obtain predicted inhibitory activity ranking against the bacterial ASADHs. This analysis was performed to prioritize the available compounds for testing. A virtual compound library of 19 compounds was examined (Fig. 5), with each compound composed of 10 different conformations created by varying the dihedral angles of each rotatable bond into their various lower energy conformers. This library was then screened by using validated docking models and a comparative analysis of docking scores was performed. The structures with the highest scores and those that showed the greatest selectivity between the two homologous enzyme forms (Table 1) were identified for kinetic testing in our assay. In addition, some of the compounds from this library were derivatized to examine the role of key functional groups.

2.2. Chemistry

Esterification of the commercially available compounds **M6**, **M7** and **M17** were carried out as depicted in Scheme 1 by refluxing in methanol in the presence of catalytic amounts of sulfuric acid. The *N*-alkyl derivatives of **M11** and **M14** were prepared as shown in Scheme 2 by deprotonation, followed by nucleophilic displacement of iodide from the alkylating reagents.

2.3. Kinetic evaluation

Based on these screening results two compounds were initially examined kinetically (entries **M9** and **M17** in Table 1) against both forms of ASADH. These compounds were selected because of their availability, high predicted inhibitory activity, and/or good predicted selectivity for at least one of the ASADHs. The docking models predicted that compound **M9** would be a fairly potent inhibitor of both bacterial ASADHs, while compound **M17** would be a more selective inhibitor of *vc*ASADH (Table 1). The predicted selectivity for **M17** against *vc*ASADH appears to be derived from an alignment of the *p*-nitrophenyl side-chain of **M17** into the additional binding pocket adjacent to the active site in only this enzyme form (Fig. 6B). Enzyme kinetic studies confirmed that each of these compounds is a good inhibitor of the ASADHs, with K_i values ranging from 110 to 180 μM (Table 1). However, no significant species selectivity was observed for either of these compounds. Despite this specific shortcoming, the virtual screening approach did successfully predict the interaction of these analogs with our target enzymes. This, in turn, led to the identification of new inhibitors that belong to more diverse chemical classes than the substrate analogs previously investigated.

To extend these initial results, four additional analogs (entries **M6**, **M7**, **M11** and **M14**, Table 1) were selected for kinetic screening because of their structural relationship to the inhibitor **M9**. While both **M9** and **M17** showed good enzyme affinity, the former compound could serve as a better lead for further development because of its higher ligand efficiency[20] (0.35 kcal/mol/heavy atom for **M9** vs 0.22 for **M17**). The analogs **M9** and **M11** differ by a single chloro substitution at position 4 in **M9**, so **M11** was chosen for screening to assess the importance of this additional substitution. The kinetic assay showed that the presence of this chloro substitution has a positive influence, leading to approximately a 10-fold increase in binding of the corresponding analog **M9** (Table 1). This enhanced affinity for the chloro-derivative (**M9** vs **M11**) is likely the result of a different type of binding interaction. The docking models show that the chloro group in **M9** interacts with β-carboxylate group of an aspartyl residue (asp230 and asp210 in *vc*ASADH and *sp*ASADH, respectively) through a 'halogen-bonding' interaction. The high polarizability of chlorine can be further potentiated by the electron withdrawing substitution on **M9**, leading to the improving binding affinity of this analog. This halogen bond is a short non-covalent C–X···O–Y type electrostatic interaction with the 'X···O' distances within the sums of van der Waals radii of the interacting atoms where the negative charge from an oxygen, nitrogen, or sulfur (acting as a Lewis base) is transferred to a polarizable halogen (acting as a Lewis acid).[21] Furthermore, a halogen bond has been found, depending on the polarizability of the halogen, to improve ligand binding with a stabilizing potential the same as that of an average hydrogen bond.[22]

M6 contains a monocarboxylate replacement of the phthalimide moiety in **M11**. Similarly, the dicarboxylate analog **M7** provided a good comparison between a nitro and a carboxylate group, allowing an assessment of their influence on binding affinity. The pair-wise comparison between **M7** and **M6** shows a twofold improvement in binding for the carboxylate versus the nitro group (Table 1). Our comparative kinetic analysis of this set of inhibitors suggests that the presence of a phthalimide moiety does not make a significant contribution to the binding profile of **M11**. However, the pyridine nitrogen in both **M6** and **M7** must play some role in binding since the 1,4-benzenedicarboxylate analog without this heteroatom has no affinity for either of the ASADHs. To examine the function of this moiety **M14** serves as a benzimidazolinone scaffold replacement of the phthalimide scaffold in **M11**, and shows a nearly 10-fold improvement in binding affinity to *sp*ASADH. Interestingly, this analog has nearly a threefold selectivity preference for the gram-positive form of ASADH, which is opposite of the predicted preference of *vc*ASADH from docking studies (Table 1).

To confirm that these inhibitors are binding as predicted in the amino acid substrate site, several compounds were selected for more thorough kinetic analysis with *vc*ASADH. The concentrations of these selected inhibitors were varied against different levels of the substrate ASA and the resulting rates were analyzed to determine the inhibition type. Both **M9** and **M14m** were found to be

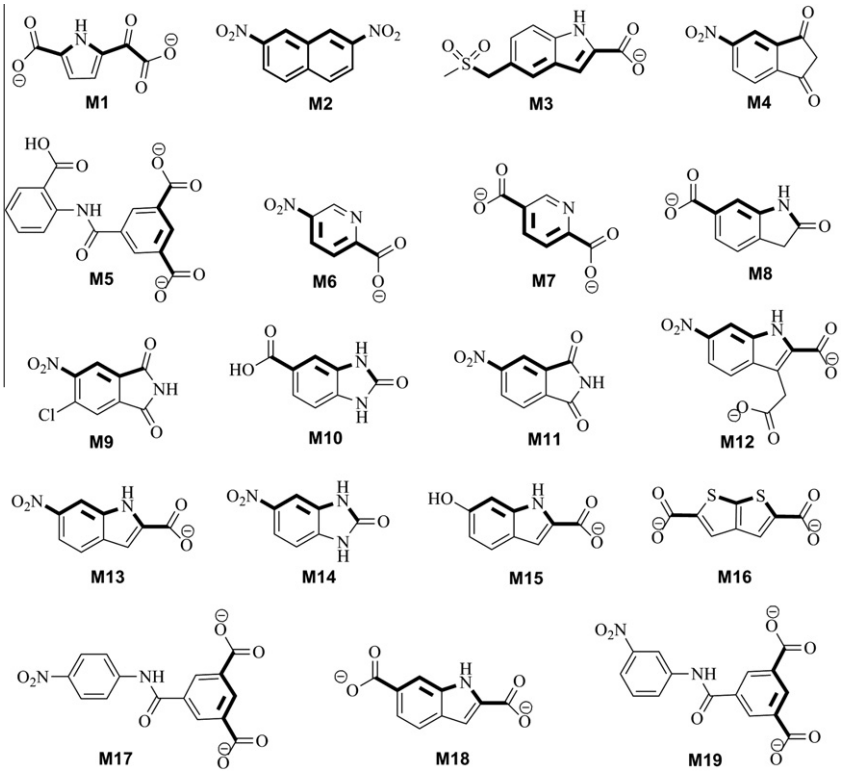

Figure 5. Library of virtual compounds each containing a substructure (bold) that can potentially form favorable interactions with the two key active site arginyl residues in ASADHs.

Table 1
Comparative analysis of the docking scores for the compound library and kinetic assay data for selected compounds (in bold)

Compound ID	*sp*ASADH		*vc*ASADH	
	Dock Score[a]	Exp. K_i[b]	Dock Score[a]	Exp. K_i[b]
M1	0.0069		0.044	
M2	0.020		0.12	
M3	0.022		1.0	
M4	0.083		0.10	
M5	0.13		0.23	
M6	**0.17**	**1.2 ± 0.2**	**2.3**	**2.1 ± 0.3**
M6m	**0.12**	**>20**[c]	**0.01**	**>20**[c]
M7	**0.20**	**0.69 ± 0.21**	**3.4**	**1.2 ± 0.3**
M7m	**0.41**	**>20**[c]	**0.26**	**>20**[c]
M8	0.25		0.65	
M9	**0.50**	**0.15 ± 0.03**	**0.022**	**0.18 ± 0.05**
M10	0.69		2.5	
M11	**0.71**	**3.3 ± 0.9**	**0.19**	**2.6 ± 0.9**
M11m	**0.005**	**0.89 ± 0.10**	**0.046**	**1.1 ± 0.3**
M11e	**0.17**	**>4**[c]	**0.08**	**>4**[c]
M12	0.74		0.98	
M13	1.3		0.52	
M14	**1.9**	**0.40 ± 0.07**	**0.030**	**1.1 ± 0.3**
M14m	**0.07**	**0.086 ± 0.030**	**0.12**	**0.13 ± 0.02**
M14e	**14.7**	**>4**[c]	**1.66**	**>4**[c]
M15	2.7		0.17	
M16	9.1		6.8	
M17	**11.7**	**0.11 ± 0.03**	**0.0033**	**0.18 ± 0.11**
M17m	0.68	**>20**[c]	0.18	**>20**[c]
M18	12.9		2.3	
M19	17.8		0.032	

[a] Predicted K_i value (in mM) for the optimal docking pose from SYBYL 8.0.
[b] K_i values (in mM) calculated from a fit to the Dixon equation[25] for competitive inhibition.
[c] No inhibition observed. K_i values were estimated to be at least 10-times the highest concentration tested.

competitive inhibitors against the substrate ASA, with K_i values of 197 ± 33 μM for **M9** and 24 ± 5 μM for **M14m**.

2.4. Examination of functional group interactions

In the absence of specific structural insights into how each of these analogs binds to the active site, their potential binding interactions were evaluated from a mechanistic viewpoint. Based on the selection criteria for these compounds and their competitive inhibition versus ASA, it is reasonable to assume that each can bind by engaging the two highly conserved active site arginines (Arg 99 and 245 for *sp*ASADH or Arg 101 and 267 for *vc*ASADH) that have been shown to bind phosphate and the ASA carboxyl group, respectively.[16] The proposed alignment to bridge these active site binding groups is highlighted in bold for each of these compounds (Fig. 5). The arginine residues, in turn, can engage with key functional groups within these analogs either through electrostatic interactions or by acting as hydrogen bond donors. Mechanistically, at physiological pH the carboxylate moieties of the inhibitors will be ionized to potentially interact with the arginines through electrostatic interactions. To test this hypothesis, the analogs **M6**, **M7** and **M17** were derivatized into their corresponding methyl esters. As predicted, the ester derivatives of these parent compounds have completely lost their affinity for both forms of ASADH, supporting the hypothesis of the requirement for these critical electrostatic interactions with the active site arginines. In addition, the complete loss of binding affinity by the ester derivatives eliminates hydrogen bonding as a possible binding mode since that mode could still be available with the ester derivatives. This further supports the assumption that electrostatic interactions are the predominant interactions in substrate (and inhibitor) recognition.

To further test the roles of the various functional groups during binding, the phthalimide **M11** and the benzimidazolinone **M14** were N-alkylated to increase the electron density on the oxygen

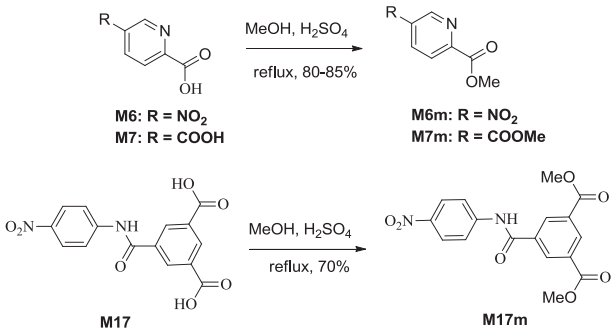

Scheme 1. Syntheses of methyl ester derivatives.

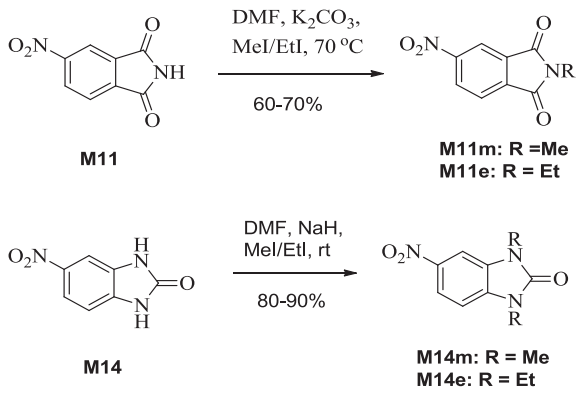

Scheme 2. Syntheses of *N*-alkyl phthalimide and benzimidazolinones derivatives.

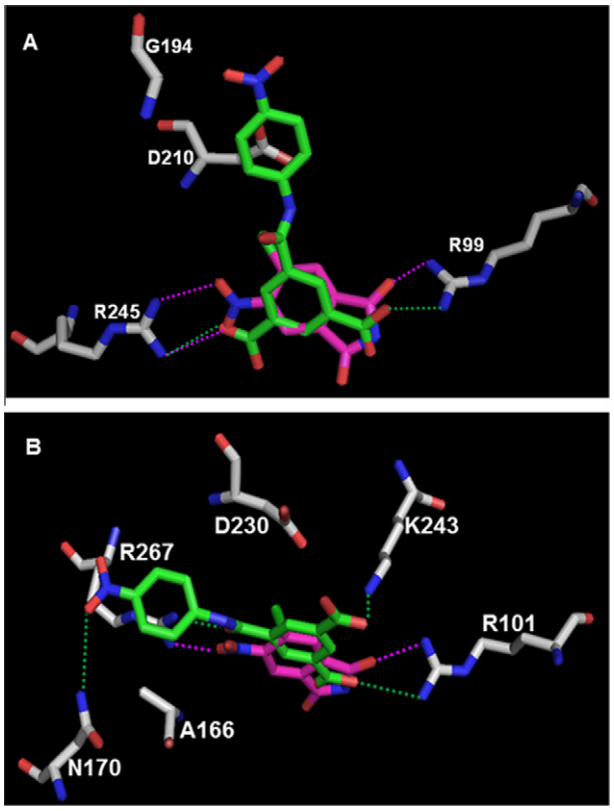

Figure 6. Surflex-Dock generated binding orientation of M17 (in green) and M9 (in magenta) within *sp*ASADH (panel A) and *vc*ASADH (panel B); Note that M9 binds with a similar mode and orientation in both enzymes, while M17 assumes a different orientation.

atoms, and to eliminate the possibility of hydrogen bonding to the NH groups. In this case, the underlying hypothesis is that these oxygens could electrostatically interact with the arginines since they would possess partial negative charges that would be further enhanced as part of the amide functionality in these structures. As expected, the affinity of the *N*-methyl derivative (**M11m)** and the *N*,*N*-dimethyl derivative (**M14m)** each improved compared to the parent compounds. The binding affinity for **M11m** increased with both forms of ASADH, by a factor of greater than two for *vc*ASADH and a factor of nearly four for *sp*ASADH. Likewise, the affinity for **M14m** improved by a factor of from 5 to 8, and still shows about a twofold preference for binding to *sp*ASADH, with experimental K_i values that are now nearly identical to the predicted values (Table 1). An alternative explanation for this improved affinity is that alkylation could lead to improved binding through enhanced van der Waals interactions. However, the corresponding *N*-ethyl (**M11e**) and *N*,*N*-diethyl (**M14e**) derivatives showed no affinity for either form of ASADH. This result suggests that if hydrophobic interactions contribute toward improving affinity, then the active site must place a severe penalty on the additional bulk present in the ethyl derivatives. Therefore, although the argument against the significant participation of van der Waals interactions is based on a very limited set of data, binding through electronic interactions with the exocyclic oxygens is the more straightforward explanation for the increased affinity upon N-alkylation.

3. Conclusions

Several new structural scaffolds have been identified that function as moderately effective inhibitors of bacterial ASADHs. While these inhibitors are quite different from the physiological substrates of our target enzyme, they each contain appropriately positioned functional groups that appear capable of making productive binding interactions with key active site amino acids.

4. Experimental

4.1. Molecular modeling and docking

All enzyme related graphics were performed by using PYMOL (release 0.99).[23] Molecular modeling and docking studies were performed using SYBYL 8.0 (Tripos, Inc.), on a Linux workstation. The SKETCH option in SYBYL was used to generate three-dimensional structures for each compound using the default settings. Gasteiger–Huckel charges were applied to the molecules after adding all hydrogen atoms before energy calculations were performed using the Tripos force-fields. The Powell conjugate-gradient algorithm with a termination criterion of 0.05 kcal/mol was used for energy minimizations. Docking was performed using the Surflex-dock™ docking package on SYBYL 8.0 that uses Hammerhead docking system based empirical scoring function and its search engine relies on a surface-based molecular similarity method.[24] The structure of ASADH with the bound inhibitor 2-aminoadipate (2-aa)[18] was used in these docking studies (Fig. 1). Various docking protocols were generated by varying the 'bloat' and 'threshold' values with/without changing mode of protomol generation such as automatic or ligand based methods. The generated docking models were validated both internally and externally before predicting the activity of a virtual library of compounds.

4.2. Data sets

To evaluate the predictions and to improve the predictability of the docking models a small set of compounds that were previously shown to inhibit ASADHs[25] were chosen as a test set (Fig. 2). For virtual screening of new potential inhibitors a small library of

commercially available molecules was examined. This library was assembled from chemical structures that can potentially maintain the key binding interactions that are present between ASADH and its substrates (i.e., aspartyl phosphate and aspartyl β-semialdehyde). Each of these chosen molecules have at least one negative charge-bearing functionality to support an electrostatic interaction with one of the active site arginyl residues, and an appropriately positioned second functional group to bridge across to the other active site arginyl residue (Fig. 3).

4.3. Synthesis

Chemical reactions were conducted under nitrogen in anhydrous solvents unless stated otherwise. Anhydrous solvents were purchased from commercial sources and were used without additional purification except for: (i) Acetone (Me_2CO) which was further dried over 3 Å molecular sieves; and (ii) tetrahydrofuran (THF) which was further distilled under nitrogen over sodium-benzophenone. All other reagents obtained from commercial suppliers were used without further purification. Thin-layer chromatography (TLC) was done on 250 μm fluorescent TLC plates (Baker-flex, Silica Gel IB-F from VWR International, LLC) and visualized by using UV light or iodine vapor. Normal-phase flash and gravity column chromatography were performed using silica gel (200–425 mesh 60 Å pore size) and ACS grade solvents. Melting points were determined on an Electrothermal digital melting point apparatus and are uncorrected. NMR spectra were recorded on either a Varian Inova-600 spectrometer at 600 MHz, or a Unity-400 spectrometer at 400 MHz. Peak locations were referenced using either tetramethylsilane (TMS) or residual nondeuterated solvent as an internal standard. ^{13}C NMR chemical shifts are reported to the first decimal place unless peaks are very close wherein for such instances values are reported to a second decimal place.

4.3.1. General esterification procedure

Synthesis of methyl ester derivatives of **M6**, **M7**, and **M17** was carried out under catalytic esterification conditions as depicted in Scheme 1. To a solution of the appropriate carboxylic acid in methanol few drops of conc. sulfuric acid were added. Subsequently, the reaction mixture was refluxed for 6–10 h. After completion, the volatile solvents were evaporated under reduced pressure and the residue was dissolved in water/ethyl acetate mixture. The aqueous phase was extracted with ethyl acetate and the combined organic phase was washed with 5% sodium bicarbonate, brine, and was dried over anhydrous sodium sulfate. After filtration the desired ester was obtained using flash column chromatography.

4.3.1.1. 5-Nitropyridine-2-methylcarboxylate (M6m). Mp = 156–159 °C; TLC R_f = 0.5 (EtOAc/hexanes (1:1)); ^1H NMR ($CDCl_3$, 600 MHz) δ 8.53 (1H, s), 8.66 (1H, dd, J = 1.8, 8.4 Hz), 8.56 (1H, d, J = 8.4 Hz), 4.08 (3H, s); ^{13}C NMR ($CDCl_3$, 150 MHz) δ 153.8, 152.1, 153.6, 145.1, 138.4, 125.5, 53.6; [M+Na]/Z = 205.3.

4.3.1.2. Pyridine-2,5-dimethylcarboxylate (M7m). Mp = 162–166 °C; TLC R_f = 0.33 (EtOAc/hexanes (1:1); ^1H NMR ($CDCl_3$, 600 MHz) δ 8.31 (1H, s), 8.45 (1H, dd, J = 1.8, 7.8 Hz), 8.22 (1H, d, J = 1.8 Hz), 4.05 (3H, s), 4.00 (3H, s); ^{13}C NMR ($CDCl_3$, 150 MHz) δ 164.9, 164.8, 151.8, 150.7, 138.3, 126.6, 124.7, 53.2, 52.3; [M+Na]/Z = 218.3.

4.3.1.3. 5-[[(4-Nitrophenyl)amino]carbonyl]-1,3-benzenedimethylcarboxylate (M17m). Mp = 225–228 °C; TLC R_f = 0.84 (EtOAc); ^1H NMR ($CDCl_3$, 600 MHz) δ 8.54 (1H, s), 8.52 (2H, m), 8.38 (2H, d, J = 8.4 Hz), 8.08 (2H, d, J = 8.4 Hz), 3.37 (3H, s); ^{13}C NMR ($CDCl_3$, 150 MHz) δ 131.5, 128.3, 125.3, 125.2, 124.1, 89.2, 52.8.

4.3.2. General procedure for N-alkylation of phthalimides

N-Methylation of phthalimide derivative **M11** was obtained by nucleophilic displacement of iodide from alkyl iodide by deprotonated phthalimide. A mixture of appropriate phthalimide, iodoalkane, and potassium carbonate in DMF was stirred for 6–10 h at 70–110 °C. After completion, the mixture was poured into an ice/water mixture. The aqueous phase was extracted with dichloromethane. The combined organic phase was washed with 0.1 HCl, brine and was dried over anhydrous sodium sulfate. The desired N-alkylated product was isolated using flash column chromatography.

4.3.2.1. 4-Nitro-N-methylphthalimide (M11m). Mp = 163–170 °C; TLC R_f = 0.54 (EtOAc/hexanes (1:1)); ^1H NMR ($(CD_3)_2O$, 600 MHz) δ 8.57 (1H, dd, J = 1.8, 8.4 Hz), 8.52 (1H, d, J = 1.2 Hz), 8.12 (1H, d, J = 8.4 Hz), 3.15 (3H, s); ^{13}C NMR ($(CD_3)_2O$, 150 MHz) δ 167.1, 166.8, 137.7, 134.6, 130.0, 125.0, 118.4, 24.4.

4.3.2.2. 4-Nitro-N-ethylphthalimide (M11e). Mp = 117–120 °C; TLC R_f = 0.66 (EtOAc/hexanes (1:1)); ^1H NMR ($CDCl_3$, 600 MHz) δ 8.62 (2H, m), 8.04 (1H, d, J = 8.4 Hz), 3.81 (2H, q, J = 7.2 Hz), 1.31 (3H, t, J = 7.2 Hz); ^{13}C NMR ($CDCl_3$, 150 MHz) δ 166.0, 165.7, 151.6, 136.6, 133.6, 129.1, 124.3, 118.5, 33.6, 13.7.

4.3.3. General procedure for N-alkylation of benzimidazolinone

Additionally, the 5-nitro-2-benzimidazolinone was N-alkylated through a sequential deprotonation and nucleophilic displacement maneuver. The benzimidazolinone was first deprotonated by using sodium hydride, which then performed a nucleophilic displacement of the iodo group upon addition of the respective alkyl iodides (Scheme 2). To a mixture of 60% NaH in DMF, a solution of nitrobenzimidazolinone in DMF was added under inert atmosphere. The resulting mixture was stirred at rt for 30 min. To this mixture appropriate iodoalkane was added. The reaction mixture was stirred at rt for 6–8 h. After completion, the reaction was quenched with 0.1 N HCl. The aqueous phase was extracted with ethyl acetate. The combined organic phase was washed with 5% sodium bicarbonate, brine and was dried over anhydrous sodium sulfate. The desired product was purified using flash column chromatography.

4.3.3.1. 4-Nitro-N,N-dimethylbenzimidazolinone (M14m). Mp = 200–204 °C; TLC R_f = 0.27 (EtOAc/hexanes (2:1)) ^1H NMR ($CDCl_3$, 600 MHz) δ 8.13 (1H, dd, J = 1.8, 8.4 Hz), 7.83 (1H, d, J = 1.8 Hz), 7.03 (1H, d, J = 8.4 Hz), 3.50 (3H, s), 3.49 (3H, s); ^{13}C NMR ($CDCl_3$, 100 MHz) δ 154.7, 142.6, 135.0, 129.9, 118.4, 106.4, 103.2, 27.6, 27.5.

4.3.3.2. 4-Nitro-N,N-diethylbenzimidazolinone (M14e). Mp = 134–138 °C, TLC R_f = 0.5 (EtOAc/hexanes (1:1)); ^1H NMR ($CDCl_3$, 400 MHz) δ 8.08 (1H, dd, J = 2.0, 8.4 Hz), 7.89 (1H, d, J = 2.0 Hz), 7.03 (1H, d, J = 8.4 Hz), 3.98 (4H, m), 1.36 (6H, m); ^{13}C NMR ($CDCl_3$, 100 MHz) δ 153.7, 142.3, 134.2, 129.0, 118.1, 106.4, 103.2, 36.36, 36.31, 13.5.

4.4. Enzymatic assay

The ASADHs from *S. pneumoniae* and *V. cholerae* were cloned, expressed, and purified following our published procedures.[26] After concentrating, the enzyme was stored at −20 °C in 50 mM HEPES (pH 7) containing 1 mM EDTA and dithiothreitol (DTT). ASADH generates an aldehyde from an acyl phosphate by reductive dephosphorylation as shown in Scheme 3. This is a reversible reaction and, because of instability of aspartyl phosphate, the reverse reaction is followed by monitoring the increase in the absorbance of NADPH at 340 nm.

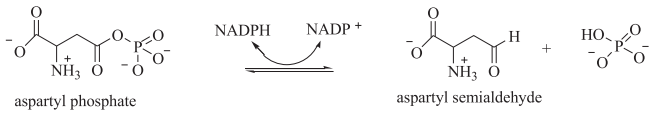

Scheme 3. Aspartate β-semialdehyde dehydrogenase (ASADH) catalyzed reaction.

Kinetic assays were carried at room temperature with a reaction mixture composed of 120 mM CHES (pH 8.6) buffer and 200 mM KCl in a 96-well plate. The substrates working concentrations of ASA, NADP, and phosphate were 1 mM, 1.5 mM, and 20 mM, respectively. The reaction was initiated by adding 30 μL of enzyme solution to the mixture of assay buffer and substrates. To determine the inhibition constant (K_i) of each inhibitor, compounds were added to each well in a particular row with the concentrations varied by serial dilution. The initial velocities were fitted to the Dixon equation[27] to determine K_i values, which assumes that each inhibitor is competitive with the substrate ASA. To obtain optimal enzyme assay conditions for DMSO soluble inhibitors, 20% DMSO was used in the reaction buffer and, as previously observed, this level of DMSO does not have any adverse effect on the activity of ASADHs.[25] For selected inhibitors a more complete kinetic analysis was conducted in which the substrates were varied at different inhibitor concentrations and the data were analyzed by fitting to standard models for different types of inhibition. In each case these compounds were found to be competitive inhibitors against ASA.

Acknowledgements

This work was supported by grant AI077720 from the National Institutes of Health. The authors thank Bharani Thangavelu (University of Toledo) for conducting the kinetic analyses of these enzyme inhibitors.

References and notes

1. Maree, C. L.; Daum, R. S.; Boyle-Vavra, S.; Matayoshi, K.; Miller, L. G. *Emerg. Infect. Dis.* **2007**, *13*, 236.
2. Viola, R. E. *Acc. Chem. Res.* **2001**, *34*, 339.
3. Galan, J. E.; Nakayama, K.; Curtiss, R. *Gene* **1990**, *94*, 29.
4. Akerley, B. J.; Rubin, E. J.; Novick, V. L.; Amaya, K.; Judson, N.; Mekalanos, J. J. *Proc. Natl. Acad. Sci. U.S.A.* **2002**, *99*, 966.
5. Salama, N. R.; Shepard, B.; Falkow, S. *J. Bacteriol.* **2004**, *186*, 7926.
6. Hadfield, A. T.; Kryger, G.; Ouyang, J.; Petsko, G. A.; Ringe, D.; Viola, R. E. *J. Mol. Biol.* **1999**, *289*, 991.
7. Blanco, J.; Moore, R. A.; Kalabeeswaran, V.; Viola, R. E. *Protein Sci.* **2003**, *12*, 27.
8. Blanco, J.; Moore, R. A.; Viola, R. E. *Proc. Natl. Acad. Sci. U.S.A.* **2003**, *100*, 12613.
9. Faehnle, C. R.; Liu, X.; Le Coq, J.; Viola, R. E. *J. Biol. Chem.* **2006**, *281*, 31031.
10. Arachea, B. T.; Liu, X.; Pavlovsky, A.; Viola, R. E. *Acta Crystallogr., Sect. D* **2010**, *66*, 205.
11. Faehnle, C. R.; Ohren, J. F.; Viola, R. E. *J. Mol. Biol.* **2005**, *353*, 1055.
12. Karsten, W. E.; Viola, R. E. *Biochim. Biophys. Acta Protein Struct. Mol. Enzymol.* **1992**, *1121*, 234.
13. Karsten, W. E.; Viola, R. E. *Biochim. Biophys. Acta* **1991**, *1077*, 209.
14. Ouyang, J.; Viola, R. E. *Biochemistry* **1995**, *34*, 6394.
15. Blanco, J.; Moore, R. A.; Faehnle, C. R.; Viola, R. E. *Acta Crystallogr., Sect. D* **2004**, *60*, 1808.
16. Blanco, J.; Moore, R. A.; Faehnle, C. R.; Coe, D. M.; Viola, R. E. *Acta Crystallogr., Sect. D* **2004**, *60*, 1388.
17. Klebe, G. *Drug Discovery Today* **2006**, *11*, 580.
18. Pavlovsky, A.; Liu, X.; Faehnle, C. R.; Potente, N.; Viola, R. E. *Chem. Biol. Drug Des.* **2012**, *79*, 128.
19. Pan, J.; Liu, G. Y.; Cheng, J.; Chen, X. J.; Ju, X. L. *Eur. J. Med. Chem.* **2010**, *45*, 967.
20. Hopkins, A. L.; Groom, C. R.; Alex, A. *Drug Discovery Today* **2004**, *9*, 430.
21. Politzer, P.; Lane, P.; Concha, M. C.; Ma, Y.; Murray, J. S. *J. Mol. Model.* **2007**, *13*, 305.
22. Auffinger, P.; Hays, F. A.; Westhof, E.; Ho, P. S. *Proc. Natl. Acad. Sci. U.S.A.* **2004**, *101*, 16789.
23. DeLano, W. L. *The PyMOL Molecular Graphics System*. DeLano Scientific: San Carlos, CA, 2002.
24. Jain, A. N. *J. Comput. Aided Mol. Des.* **2007**, *21*, 281.
25. Gao, G.; Liu, X.; Pavlovsky, A.; Viola, R. E. *J. Biomol. Screen.* **2010**, *15*, 1042.
26. Moore, R. A.; Bocik, W. E.; Viola, R. E. *Protein Expr. Purif.* **2002**, *25*, 189.
27. Dixon, M. *Biochem. J.* **1953**, *55*, 170.